2003

The Variability of Currents in the Yucatan Channel: Analysis of Results from a Numerical Ocean Model

Tal Ezer
Old Dominion University, tezer@odu.edu

Lie-Yauw Oey

Hyun-Chul Lee

Wilton Sturges

Original Publication Citation

Ezer, T., Oey, L.Y., Lee, H.C., & Sturges, W. (2003). The variability of currents in the Yucatan Channel: Analysis of results from a numerical ocean model. *Journal of Geophysical Research C: Oceans, 108*(1), 1-13. doi: 10.1029/2002JC001509

JOURNAL OF GEOPHYSICAL RESEARCH, VOL. 108, NO. C1, 3012, doi:10.1029/2002JC001509, 2003

The variability of currents in the Yucatan Channel: Analysis of results from a numerical ocean model

Tal Ezer, Lie-Yauw Oey, and Hyun-Chul Lee
Program in Atmospheric and Oceanic Sciences, Princeton University, Princeton, New Jersey, USA

Wilton Sturges
Department of Oceanography, Florida State University, Tallahassee, Florida, USA

Received 12 June 2002; revised 27 August 2002; accepted 3 September 2002; published 18 January 2003.

[1] The flow through the Yucatan Channel and into the Gulf of Mexico is a major component of the Gulf Stream and the subtropical gyre circulation. Surprisingly, however, little is known about the forcing and physical parameters that affect the current structures in the Channel. This paper attempts to improve our understanding of the flow through the Channel with a detailed analysis of the currents obtained from a primitive-equation model that includes the Gulf and the entire Caribbean Sea and forced by 6-hourly wind from ECMWF. The analysis includes two parts: First, the overall statistics of the model results, including the Loop Current (LC) variability, the frequency of LC eddy-shedding, and the means and standard deviations (SD) of transports and currents, are compared with observations. Secondly, an Empirical Orthogonal Function (EOF) analysis attempts to identify the physical parameters responsible for the dominant modal fluctuations in the Channel. The model LC sheds seven eddies in 4 years at irregular time intervals (6.6, 7.1, 5.3, 11.9, 4.2, 10.9 months). The model's upper (thickness $\sim$800 m) inflow into the Gulf of Mexico occupies two-thirds of the Channel on the western side, with a near-surface maximum (4-year) mean of around 1.5 m s^{-1} and SD $\approx$ 0.4 m s^{-1}. Three (return) outflow regions are identified, one in the upper layer (thickness $\sim$600 m) on the eastern third of the Channel, with mean near the surface of about 0.2 m s^{-1} and SD $\approx$ 0.14 m s^{-1}, and two deep outflow cores, along the western and eastern slopes of the Channel, with (Mean, SD) $\approx$ (0.17, 0.05) and (0.09, 0.07) m s^{-1}, respectively. The total modeled Channel transport varies from 16 to 34 Sv (1 Sverdrup = 10^6 m^3 s^{-1}) with a mean around 25 Sv. The above velocity and transport values agree quite well with observations by *Maul et al.* [1985], *Ochoa et al.* [2001], and *Sheinbaum et al.* [2002]. The deep return transport below 800 m was found to correlate with changes in the Loop Current extension area, in agreement with the observational analysis by *Bunge et al.* [2002]. The EOF mode#1 of the along-channel currents contains 50% of the total energy. It is surface-trapped, is 180° out of phase across the channel, and correlates well (correlation coefficient $\gamma \approx 0.8$) with the cross-channel vacillations of the LC frontal position. The EOF mode#2 contains 18% of the energy, and its structure mimics that of the mean flow: dominated by two vertically more coherent regions that are 180° out of phase across the Channel. The mode is dominated by two periods, approximately 11 months and 2 months respectively, and correlates ($\gamma \approx 0.7$) with the upper-channel inflow transport. The third and fourth modes, together, account for 18% of the total energy. Their combined time series correlates ($\gamma \approx$ 0.66) with the deep current over the sill, and is dominated by fluctuations with a period $\approx$205 days coincident with the dominant low-frequency fluctuations inherent in *Maul et al.*'s [1985] sill measurement. Thus the dominant mode of flow fluctuations in the Yucatan Channel is caused by LC cross-frontal movements which may not be directly related to LC eddy-sheddings, while higher modes correspond to transport fluctuations that affect eddy-sheddings, and to bottom-trapped current fluctuations, the cause of which has yet to be fully uncovered. *INDEX TERMS:* 4255 Oceanography: General: Numerical modeling; 4512 Oceanography: Physical: Currents; 4520 Oceanography: Physical: Eddies and mesoscale processes; *KEYWORDS:* Yucatan Channel, numerical modeling, Gulf of Mexico, Loop Current

0148-0227/03/2002JC001509

Citation: Ezer, T., L.-Y. Oey, H.-C. Lee, and W. Sturges, The variability of currents in the Yucatan Channel: Analysis of results from a numerical ocean model, *J. Geophys. Res.*, *108*(C1), 3012, doi: 10.1029/2002JC001509, 2003.

1. Introduction

[2] The Yucatan Channel (YC) connects the Caribbean Sea with the Gulf of Mexico. As part of the North Atlantic circulation, flow from the subtropical gyre enters the Caribbean Sea and into the Gulf of Mexico, to form the Loop Current (LC), which then exits through the Florida Straits (FS) (Figure 1). Except for the relatively small water mass exchange through river runoffs and surface buoyancy fluxes, the transport in and out of the Gulf of Mexico, about 28 Sv (1 Sverdrup = 10^6 m^3 s^{-1}) [*Schmitz and Richardson*, 1991; *Schmitz and McCartney*, 1993; *Johns et al.*, 2002], is controlled by inflow through the YC and outflow through the FS. While the sill depth at the YC is about 2000 m depth, the FS is much shallower at about 800 m. Therefore, it has been suggested [e.g., *Maul*, 1977] that if there exists a deep transport in the YC below the sill depth of the FS, it must be balanced by excess inflow transport in the upper layers that accounts for variations in the volume of the LC as it extends and shed eddies into the Gulf. This would imply that variations in the deep layers are correlated with variations in the LC. However, attempts by *Maul et al.* [1985] to find a relation between the LC and the deep flow in the YC, were unsuccessful. Despite the potential importance of the YC transport as the principal driver of the LC, its likely relation to the LC eddy-shedding process, and as the major flow conduit that feeds the mighty Gulf Stream, it is surprising that since Maul's study, almost two decades elapsed before the extensive measurements of *Bunge et al.* [2002], *Ochoa et al.* [2001], and *Sheinbaum et al.* [2002] in the Channel. These recent observations cast new light into the detailed velocity structures in the Channel, and explain why the early observations by Maul over the sill did not show the expected correlation of flow with the LC. Specifically, the new observations show that most of the return deep flow is found along the eastern and western slopes of the YC and not in the middle of the sill as was previously thought. Moreover, the deep transports from the new observations do agree with the hypothesis set forth by Maul and are correlated with the variations in the LC [*Bunge et al.*, 2002].

[3] Perhaps in part due to the lack of observations prior to the more recent ones cited above, models of the Gulf tend to avoid direct reference to the dynamics of the YC [e.g., *Sturges et al.*, 1993; *Welsh and Inoue*, 2000]. This is understandable for early models, as for example in the pioneering work of *Hurlburt and Thompson* [1980], in which the prime objective was to gain a deeper understanding of the processes of LC eddy-shedding, propagation and decay inside the Gulf. Indeed, Hurlburt and Thompson's explicit specifications of transport at YC preclude a direct dynamical study of the free interaction that must exist between the LC in the Gulf and the Yucatan inflow from the Caribbean Sea. On the other hand, even in this simplified model setting, Hurlburt and Thompson's study was able to demonstrate the sensitivity of the eddy-shedding process to details of the YC-inflow profile they specified. In part inspired by Hurlburt and Thompson's work, *Oey* [1996] emphasized the importance of the interaction between the Gulf and the Caribbean Sea, and found significant outflow (fluctuations) in the deep layers in YC that correlate with inflow near the surface, as well as with episodes of LC eddy-shedding. However, Oey's work stops short of clarifying the details of these relations, the spatial and temporal structures of the velocity profiles across the Channel, as well as the natures of the forcing that produce the fluctuations. *Murphy et al.* [1999] also show the connectivity of Caribbean Sea eddies and variability in the Gulf, but unlike our study (see later) they could not find a significant correlation between LC eddy-shedding and transport variations in the YC.

[4] In this paper, we study in more details the spatial and temporal structures of flow across the Yucatan Channel, using a model (the Princeton Ocean Model, POM, see section 2 for details) that has double the grid resolution of that used by *Oey* [1996] (10 km in the Channel versus 20 km), and an expanded domain that includes the entire Caribbean Sea (instead of the northwestern portion of it), as well as the Gulf. The finer grid now results in a maximum four-year mean inflow speed of about 1.5 m s^{-1} (see below) at the Channel, a value that is more consistent with that observed [*Ochoa et al.*, 2001; *Sheinbaum et al.*, 2002]. The expanded domain eliminates any ambiguity that might result in the interpretations of the Channel's dynamics because of uncertainty in the upstream boundary conditions in a more limited Caribbean Sea domain. Our primary objectives are to describe flow structures across the Channel, and to relate them to LC variability and LC eddy-shedding events. On a more limited basis, we will also attempt to relate the model results to observations.

[5] The paper is organized as follows: First, the numerical model is briefly described in section 2, then the model results are described in section 3, and finally, a summary and conclusions are offered in section 4.

2. The Numerical Model

[6] The northwest Atlantic Ocean model used here is detailed in *Oey and Lee* [2002] and also in *Wang et al.* [2003]. The simulation is from one of the experiments detailed in L.-Y. Oey and H.-C. Lee, External forcings that influence the irregular eddy shedding from the loop current, manuscript submitted to *Journal of Geophysical Research*, 2002. The model is based on the Princeton Ocean Model (POM) [*Blumberg and Mellor*, 1987]. Vertical mixing in the model is based on the Mellor-Yamada turbulence scheme [*Mellor and Yamada*, 1982]; horizontal diffusion is based on the velocity- and grid size-dependent Smagorinsky scheme [*Smagorinsky*, 1963] with a Smagorinsky coefficient of 0.1 [for a detailed sensitivity study of the effect of this coefficient on GOM simulations, see *Oey*, 1996]. The model domain, 55°W–98°W and 5°N–50°N, includes the Gulf Stream, the Gulf of Mexico and the Caribbean Sea; fixed total inflow and outflow transports are specified across 55°W (see inset in Figure 1). These transports determine the depth-integrated velocities at the boundary, and are meant to

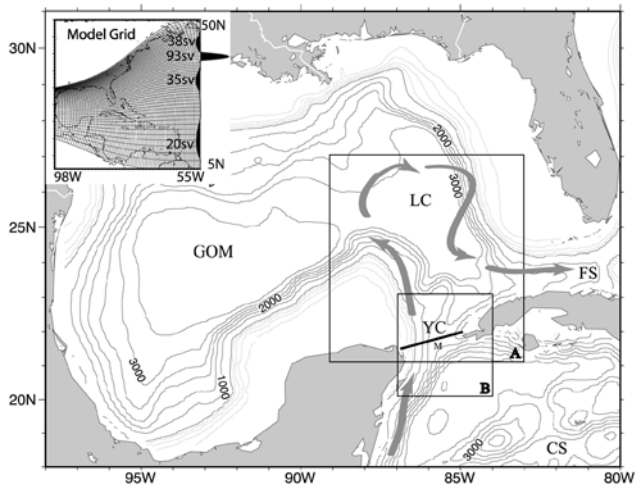

Figure 1. Bottom topography and main features of the study area. Topographic contour interval is 100 m for areas shallower than 500 m and 500 m elsewhere. The Caribbean Sea (CS), the Gulf of Mexico (GOM), the Loop Current (LC), the Florida Straits (FS) and the Yucatan Channel (YC) are indicated. The location of the *Maul et al.* [1985] observed time series of Figure 2 is marked by "M"; the cross section of Figure 4 is marked by the solid line. Region A indicates the area in which sea surface height is shown in Figure 5; region B indicates the area in which velocities are shown in Figure 6. The inset in the upper left corner shows the curvilinear model grid (every 7th grid line is shown) and the imposed boundary transports.

account for the large-scale transports (Svedrup + thermohaline) through 55°W. The three-dimensional velocity, temperature and salinity fields at the open boundary are calculated according to *Oey and Chen* [1992]. The temperature and salinity fields are advected using one-sided difference scheme when flows are eastward (that is, outflow), and are prescribed from the Generalized Digital Environmental Model (GDEM) monthly temperature and salinity climatology [*Teague et al.*, 1990] when flows are westward. These open-boundary specifications also set the baroclinic structure, which in the present case is largely geostrophic through the thermal-wind balance. The prescribed open boundaries are sufficiently removed from the Gulf of Mexico that there is a free dynamical interaction between the Caribbean Sea and the Gulf through the Yucatan Channel [*Oey*, 1996]. Horizontal resolution of the curvilinear orthogonal grid ranges from about 10 km in the vicinity of the YC to about 5 km on the northern continental shelf. There are 25 vertical sigma levels, with higher resolution near the surface and near the bottom, so that wind-driven and bottom-trapped topographic Rossby waves [*Oey and Lee*, 2002] can be better resolved. Surface forcing includes wind stress in 6-hour intervals obtained from the European Center for Medium range Weather Forecast (ECMWF) and surface heat flux and buoyancy forcing based on relaxation to monthly climatology (for sensitivity studies of the effect of surface forcing on the model simulations, see Oey and Lee, submitted manuscript, 2002). Though the full model can incorporate data assimilation that use satellite-derived sea surface temperature and altimeter data [*Wang et al.*, 2003], this study only analyzes 4 years (1993–1996) of the wind-driven model without the assimilation, following a 1-year spin up period initialized from the GDEM climatology. This allows us to study the natural variability of the model dynamics. One should keep in mind, however, that in regions with intense mesoscale activity such as in the Gulf of Mexico, the time-evolution of a model without data assimilation may not generally correspond to that observed at the same time.

3. Model Results

3.1. The Yucatan Channel Velocity, Transport, and Variations in the Loop Current Extension

[7] Until recently, our knowledge of the deep flow in the Yucatan Channel was largely based on the 1977–1980 current-meter observations just above the sill at 1895 m reported by *Maul et al.* [1985] [see also *Burkov et al.*, 1982]. While we cannot directly compare the model result with those measurements (because of different time periods and lack of data assimilation in the simulations analyzed here), it is useful to compare the means and standard deviations (SD) over a three-year period as in the observed record (Figure 2). The figure shows that both model and observation give a southwestward mean flow, though the model's southward component is more intense. Of interest is that the model has attained the observed level of

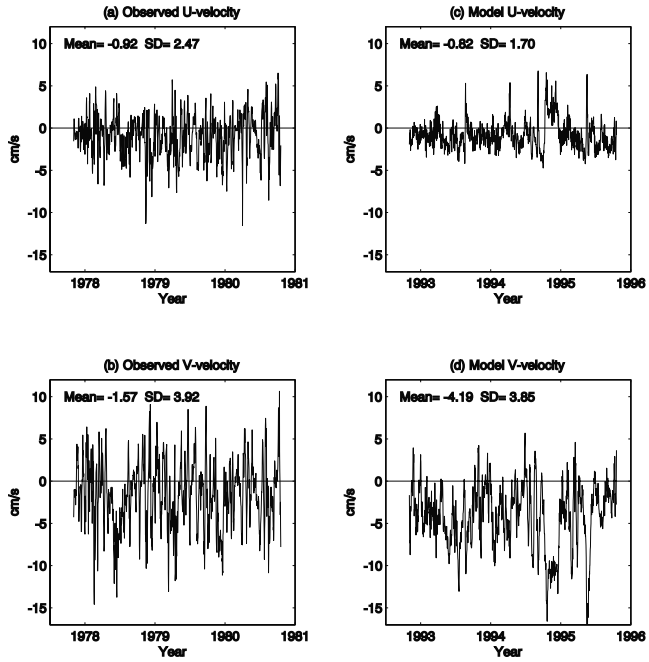

Figure 2. Comparison between the observed flow above the sill of the Yucatan Channel, at 1895 m depth [*Maul et al.*, 1985], (left panels), and model calculations (right panels). Across channel (east-west, *u* component) and along channel (north-south, *v* component) are shown in the upper and lower panels, respectively; average and standard deviation are indicated in each panel. Observed daily averages are shown from November 1977 to October 1980, and model daily averages are shown from November 1992 to October 1995.

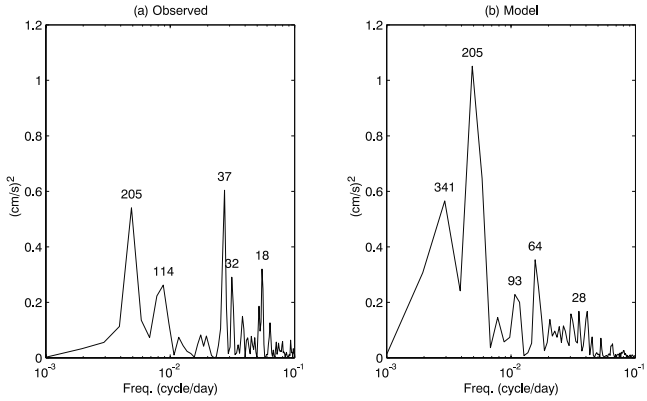

Figure 3. Power spectra of, (a) observed, and (b) model, v component records of Figure 2. The periods (in days) of the most energetic peaks are indicated.

variability especially in the along-channel component (SD $\approx$ 0.04 m s^{-1} in both model and observation). The modeled cross-channel SD is 30% less than observed, which indicates that the modeled currents are more constrained by bottom topography. Spectral analysis of the *v* component of the flow from the observations and from the model (Figure 3) reveals that both records have high frequency oscillations, as well as longer-term fluctuations (the 2 largest peaks in each figure are significant at the 95% confidence level). On the low-frequency portion, of particular interest is the occurrence of 205-day peak in both the model and observed records. We will later show that this corresponds to higher modal fluctuations in the currents. There is also a 341-day peak in the model's spectra; this we will show to correspond to the low-frequency modulation of the transport time series. For periods $\approx$ 114 days and shorter, the observation is more energetic than the model. There is some evidence in the model that the shorter-period (<114 days) fluctuations are topographic Rossby waves, in that the steep bottom slope and value of stratification support such waves with periods as short as 10 days, and that energy intensify near the bottom (not shown [c.f. *Oey and Lee*, 2002]), though clearly a detailed study in conjunction with observations is necessary to confirm the existence of these waves.

[8] The spatial structure of the mean and standard deviation of the along channel (*v* component) flow are shown in Figure 4. The section is near 21.95°N, slightly north of the Maul's current meter location (Figure 1), thus the flow at the center of the sill in this section is not the same as in Figure 2. The model has 20 horizontal grid points across the Channel (grid size $\approx$ 10 km), so the flow field is resolved quite well and in fact compared quite well with observations. However, small scale variations in the bottom topography seen in the observed sections [*Ochoa et al.*, 2001; *Sheinbaum et al.*, 2002] are not resolved. The mean flow is characterized by several cores of local maxima in flow speed. The core of the inflow into the Gulf is at 3 m depth on the western side of the Channel and has a maximum mean flow of 1.48 m s^{-1} and SD of 0.23 m s^{-1}. An outflow core on the eastern side of the Channel at $\sim$30 m depth has maximum mean flow of -0.25 m s^{-1} and SD of 0.14 m s^{-1}. This return flow is more extended and stronger (by about a factor of two) in the model than it is in the observations [*Ochoa et al.*, 2001; *Sheinbaum et al.*, 2002]. The core of the deep outflow on the western side of the Channel at 1300 m depth has mean flow of -0.17 m s^{-1} and SD of 0.05 m s^{-1}, in good agreement with the observed deep flow of about 0.2 m s^{-1} [*Ochoa et al.*, 2001]. The core of the outflow on the eastern side of the Channel at 1400 m depth has mean flow of -0.09 m s^{-1} and SD of 0.07 m s^{-1}, compared with observed outflow at that location of $\sim$0.05 m s^{-1} [*Sheinbaum et al.*, 2002].

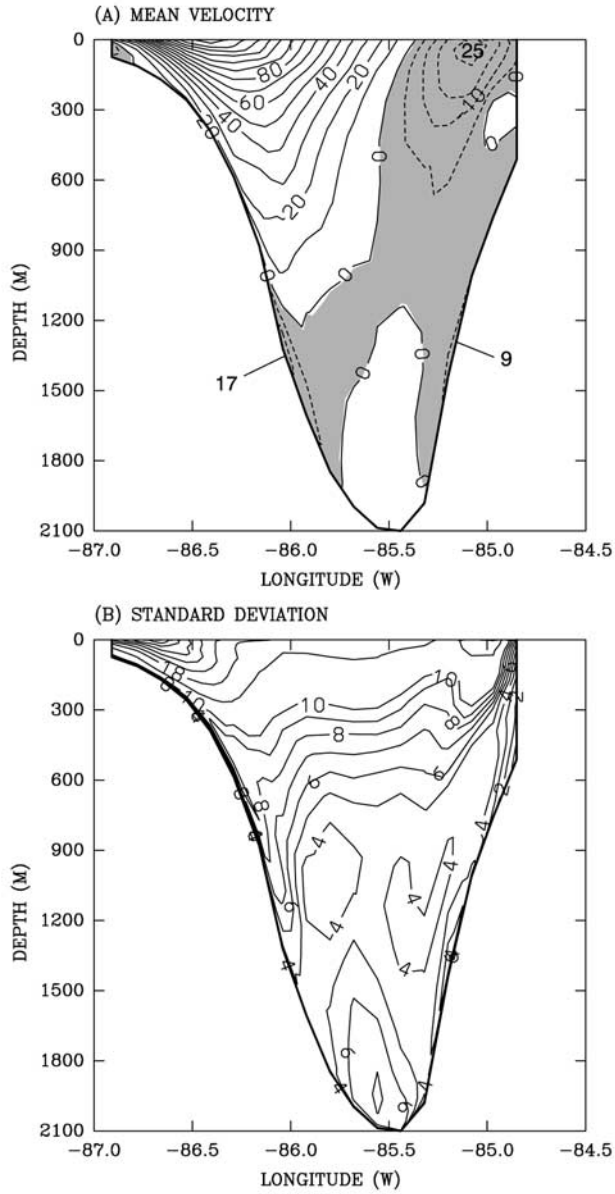

Figure 4. (a) Mean v-component velocity across the section shown in Figure 1, and calculated from the model simulations of 1993–1996. Shaded region and dashed lines indicate negative values, i.e., from the Gulf into the Caribbean Sea. (b) Standard deviation across the Yucatan Channel. Contour intervals are 0.05/0.1 m s^{-1} in (a) for negative/positive values, and 0.01/0.04 m s^{-1} in (b) for values below/above 0.1 m s^{-1}.

Another deep core has a northward velocity (inflow), and is located about 150 m above the center of the sill (the maximum of this core is 0.09 m s^{-1}, less than the first positive contour, so it is not clearly indicated in Figure 4a). The latter flow at the center of the sill seems to contrast with the deep flow in Figure 2 which is southwestward. The flow shown in Figure 2, however, is at a location (Maul's current meter) about 25 km south west of the section shown in Figure 4 (see Figure 1); the spatial structure of the near-bottom flow, discussed later, will explain the abrupt change in bottom flow direction. The highest variability of the flow is at the edge of the inflow, near the Yucatan shelf (Figure 4b), and is associated with temporary east-west shift in the inflow core, as will be shown in more detail later. The variability of the deep flow is of similar magnitude as the mean flow.

[9] The nature of the thermohaline overturning circulation and the deep water mass formation in the Gulf are not well known yet. However, close examination of the near bottom flow field reveals that a possible source for the deep outflow in the Channel is a western boundary-like near-bottom cyclonic current that hugs the slopes of the GOM at around 1500 m depth.

[10] The variations in the flow and their relation to changes in the LC, during a three-month period (October, 1995 to January, 1996) when an eddy was shed, are demonstrated in Figure 5. While the LC is growing, the return flow near the surface on the eastern side and on the deep slopes intensifies and occupies a growing portion of the Channel (Figures 5a–5c). But as the eddy shedding develops (Figures 5d–5f), the inflow core near the surface moves offshore (eastward), which causes a reduction in the return flow on the east side and an increase in the return flow on the western slope of the Channel. Note that throughout this event, the deep flow at the center of the Channel is into the Gulf, and therefore does not account for the return flow as one might perhaps expect (see below). There are similarities between this particular period and other eddy shedding events but also some differences. Not every eddy shedding event is accompanied by offshore shift in the inflow. In any case, this example demonstrates the complicated nature of the variability of the flow in the Yucatan Channel, and the fact that the position and strength of the deep return flows vary with changes of the upper inflow core.

[11] We further look at the flow field near the surface and near the bottom (Figure 6 and Figure 7) during two distinct states, corresponding to Figure 5c and Figure 5e, respectively. Though only 40 days separate between the two periods, the surface and bottom flow fields are completely different. During the first period, just before the eddy was separated from the LC, the surface inflow hugs the western side of the YC and then splits into a portion that follows the LC (north and out of the shown region) and a portion that forms the return flow on the eastern side of the YC (Figure 6a). After the eddy was separated, the surface inflow core moves offshore to the center of the Channel, and the southward recirculation occurs only south of the sill (Figure 7a), thus no apparent eastern outflow is seen in Figure 5e. The deep flow on the western slope is mostly northward during the first period (Figure 6b), but is reversed to form a southward return flow during the second period (Figure 7b). Note however, that a large part of the deep southward flow in Figure 7b turns northeastward near the center of the sill and recirculates back into the Gulf. The location of the Maul's current meter in the center of the sill is very close to the point where the deep flow turns and thus does not represent the core of the deep outflow. This recirculation pattern of the deep flow near the center of the sill explains the discrepancy in flow direction between Figure 2 and Figure 4.

[12] The variations in the YC flow and in the LC extension in the model are summarized in Figure 8. Figure 8a shows time series of variations of the LC extension, defined here as the area averaged sea surface elevation over the $6^\circ \times 6^\circ$ region-A shown in Figure 1. The approximate time of eddy shedding events is also shown. The transport through the YC is divided into three parts according to the spatial structure of the flow as shown in Figure 4: (1) the total inflow transport into the Gulf (Figure 8b, solid line), (2) the surface (above 800 m) outflow back into the Caribbean Sea (Figure 8c, dashed line), and (3) the deep outflow (below 800 m), which is dominated by the west and east slope flows (Figure 8c, solid line). The net total transport in the Channel (i.e., the sum of (1), (2) and (3) above) is also shown (Figure 8b, dashed line). Near the time of eddy shedding events, there is often a strong inflow, but also a strong return flow. As in *Oey* [1996, Figure 6a], there is an anti-correlation between the transport in the upper layers and the transport in the lower layers, which suggests that, since Oey's model domain includes only the north western portion of the Caribbean Sea, the flow is primarily controlled by local dynamics. Analysis of observations shows similar pattern [*Sheinbaum et al.*, 2002]. Unlike the transport of the Florida Current, which is dominated by the annual cycle, with a range of about 4–5 Sv [*Baringer and Larsen*, 2001], in the Yucatan Channel the annual cycle is not apparent in the model and the variability is dominated by LC extension and eddy shedding events. The total transport across the Channel in the model is 25.3 Sv, with SD of 3.2 Sv and a range between 16 to 34 Sv; these values are in good agreement with recent observed estimates of a mean transport of 25 Sv and a range between 20 to 31 Sv [*Ochoa et al.*, 2001]. However, previous studies cited a larger mean transport of 28–30 Sv [*Schmitz and Richardson*, 1991; *Schmitz and McCartney*, 1993; *Johns et al.*, 2002]. The discrepancy between different estimates can be partly explained by the large range in the net transport (Figure 8b) and by inter-annual variations. Moreover, long-term variations in the Gulf Stream transport and the subtropical gyre circulation [*Sturges and Hong*, 2001; *Ezer*, 2001] can affect the YC transport as well. This implies that a very long multiyear observed record is needed in order to accurately estimate the mean transport. The return southward flow in the model includes the upper mean transport and SD of -5.5 ± 2.5 Sv, and the bottom mean transport and SD of -2.5 ± 1.3 Sv, for a total return flow of 8 Sv. Fortuitously perhaps, the observed estimate of *Ochoa et al.* [2001] is also of 8 Sv total return transport. The inflow model transport of 33.4 ± 3.3 is also in good agreement with the observed estimate of 33 Sv [*Ochoa et al.*, 2001].

[13] Following the hypothesis [*Maul et al.*, 1985; *Bunge et al.*, 2002] that the deep return flow (solid line in Figure 8c) is related to changes in the LC extension (Figure 8a) we

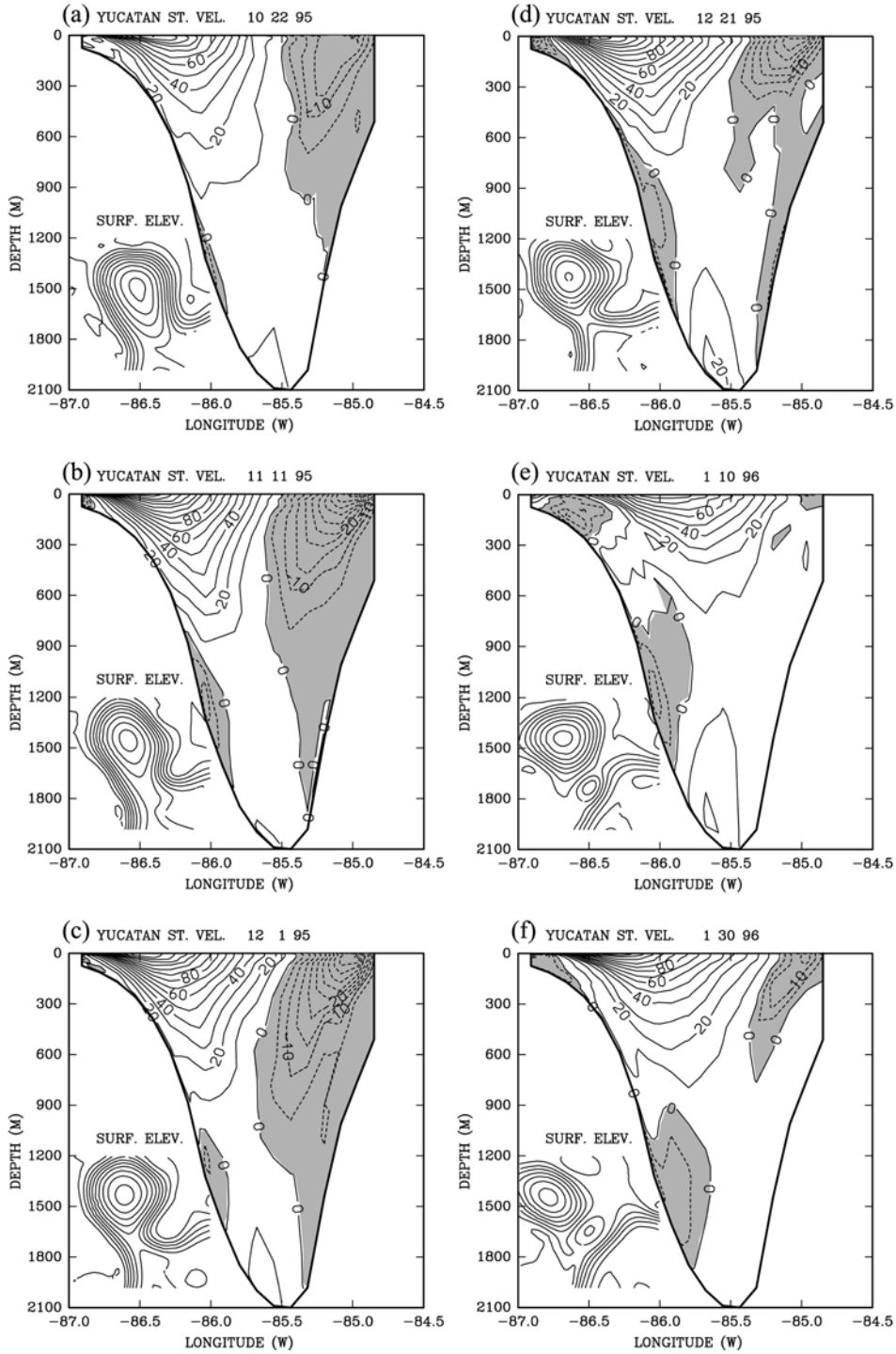

Figure 5. Along-channel velocity during an eddy shedding event; contours and shading are as in Figure 4a. Surface elevation contours in region A of Figure 1 are shown in the left-bottom corner of each panel. Figures 5a–5f are daily averages in 20-day intervals.

note that periods with relatively more deep return flow (e.g., 1996.2–1996.5) are often followed by increase in the LC extension, and these events occur usually, but not always, before or during eddy shedding events. Some large changes in LC extension, especially those with a long term nature, do not seem to relate to changes in the deep flow. Therefore, linear regression indicates small correlations between the deep flow and the LC extension itself in Figure 8. However, the deep transport is correlated to changes in the LC extension, since growing or receding LC is balanced by additional inflow and outflow transports; such a relation has been found in observations [*Bunge et al.*, 2002]. Therefore, as an indicator for the change in the LC extension we define here the derivative of the area averaged elevation, $\partial\langle\eta\rangle/\partial t$, and express it in cm sea level change per day. Figure 9 shows $\partial\langle\eta\rangle/\partial t$ together with the deep transport of Figure 8c.

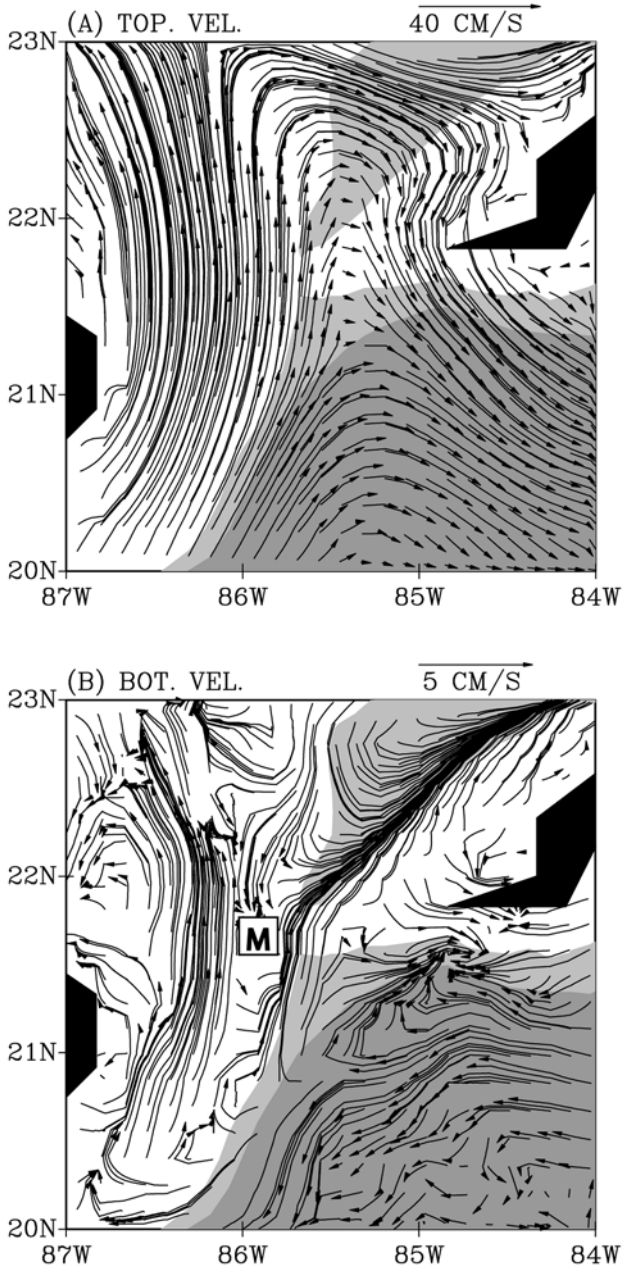

Figure 6. Daily averaged velocity vectors (in region B of Figure 1) on model day 1 December, 1995 (corresponding to Figure 5c): (a) velocity at the sixth sigma level from the surface (over the YC sill this level is at a depth of about 65 m), and (b) velocity at the sixth sigma level from the bottom (over the YC sill this level is about 65 m from the bottom). Light and dark gray shading represent bottom depths of 2000 m–3000 m and greater than 3000 m, respectively. The location of the Maul's current meter is indicated by "M".

Since the derivatives are noisy, both the sea level change and the deep transport records have been smoothed with a 30-day loss-pass filter. While the correlation coefficient between the deep transport and the LC extension was less than 0.1, the correlation coefficient has increased to 0.4 (99% confidence level) for the relation with LC changes. Thus for most peaks in $\partial\langle\eta\rangle/\partial t$ (i.e., indicating growing LC) there are counterpart peaks in the return transport. Therefore, Figure 9 corroborates the hypothesis of *Maul et al.* [1985] and the observations of *Bunge et al.* [2002] and *Sheinbaum et al.* [2002].

3.2. Empirical Orthogonal Function (EOF) Analysis of the Yucatan Channel Flow Field

[14] To get a better understanding of the spatial structure and temporal variability of the flow, Empirical Orthogonal Functions (EOF) analysis [e.g., see *Bretherton et al.*, 1992] is conducted for the along channel (south-north) velocity field. The spatial structures of the first 4 EOF modes are shown in Figure 10, the temporal evolutions of those modes are shown in Figure 11, and the power spectra of the modes

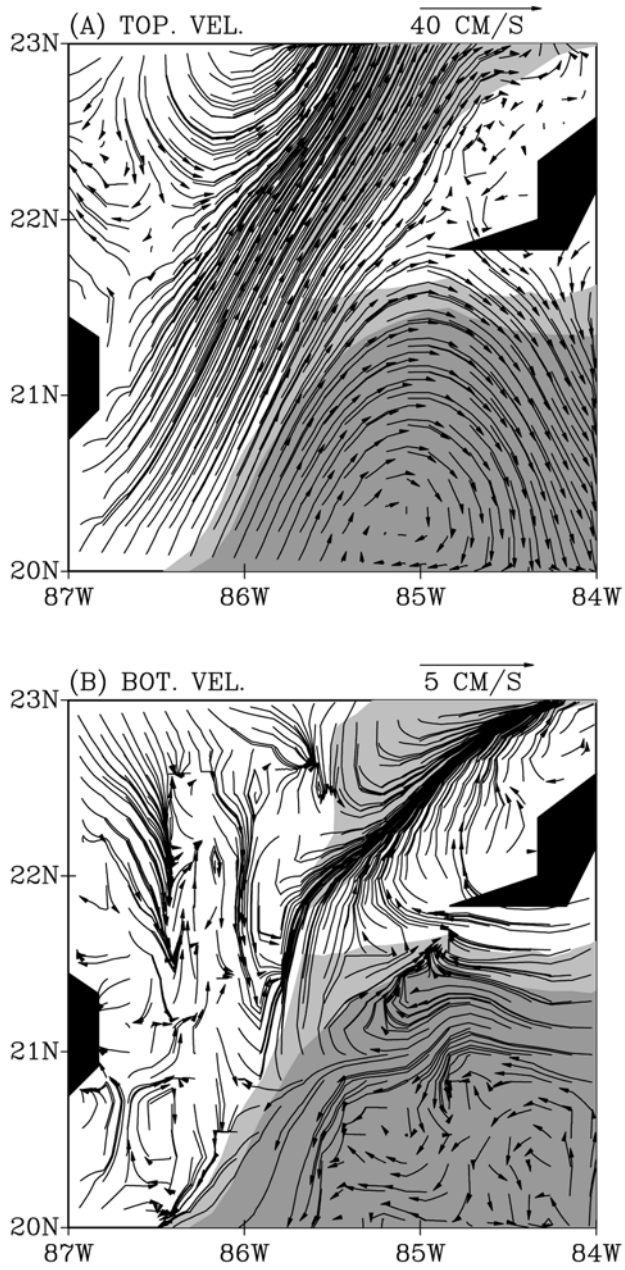

Figure 7. Velocity vectors as in Figure 6, but for model day 10 January 1996 (corresponding to Figure 5e).

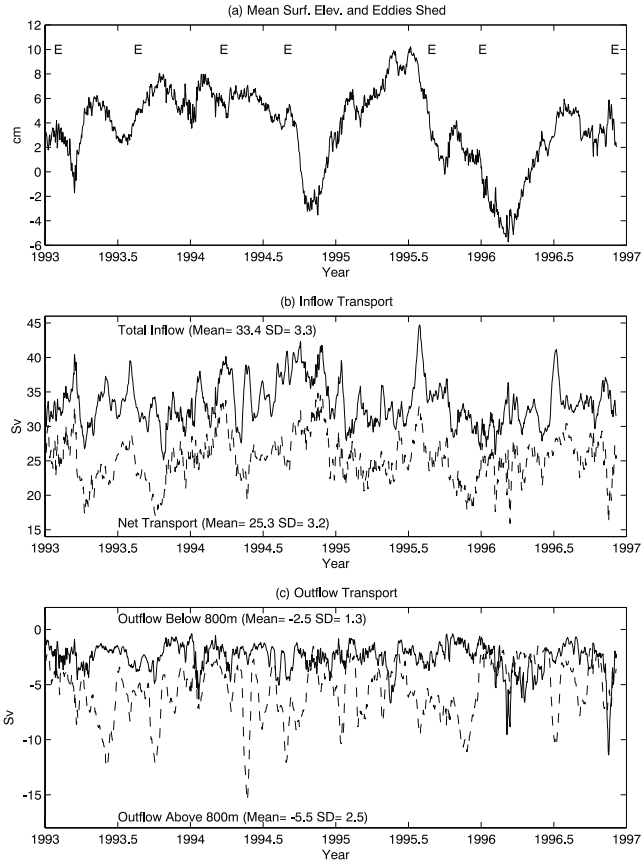

Figure 8. (a) Variations of area averaged surface elevation over the Loop Current (region A in Figure 1) and eddy shedding events (marked by "E"). (b) Variations of daily total inflow transport into the GOM (solid line), and net transport across the YC (dashed line). (c) Variations of daily outflow transport below 800 m (solid line) and outflow transport above 800 m (dashed line).

are shown in Figure 12. The first mode (which contains 50% of the variability) has the characteristic of a trapped near-surface (300–400 m) western boundary current which is out of phase with the flow to the east. The temporal evolution (Figure 11a) shows episodic events which occur about five times in four years. One example of such an event in late 1995 and early 1996 coincides with an offshore shift in the position of the inflow and the shedding of an eddy, as shown in Figure 5. The relation of the other episodes to eddy shedding events is not always clear (more discussion on this issue will come later). The most energetic peak in mode 1 is at 171 days (Figure 12a). The second EOF mode (which contains about 18% of the variability) is more vertically coherent (extends to $\sim$1000 m) and is similar in its spatial structure to the mean flow (Figure 4a). Its time evolution (Figure 11b) shows mostly high frequency variations on top of a long-term signal. The most energetic peak of mode 2 is at 341 days. The third and fourth EOF modes (which contain about 10% and 7% of the variability, respectively) involve a node at the center deep part of the YC, which is out of phase with flows on the eastern and western slopes. This spatial pattern can also be seen in the variations of the deep recirculation pattern shown in Figures 5–7. Note that, the spatial structure and the time evolution of modes 3 and 4 are in opposite phase with respect to each other. Note also, that, mode 4 is the only mode with significant variability near the bottom at the center of the sill. The most energetic peaks of modes 3 and 4 are at 256 and 171 days, respectively.

[15] The most energetic peaks in the EOF modes are at periods of 171 days (5.6 months, mode 1 and mode 4), 256 days (8.4 months, mode 1 and mode 3) and 341 days (11.2 months, mode 2 and mode 4). During the four-year period analyzed here, seven LC eddies were shed at irregular time intervals (see Figure 8a) of 6.6, 7.1, 5.3, 11.9, 4.2 and 10.9 months, thus suggesting that there may be some relation between the EOF modes and eddy shedding events. The irregular eddy shedding intervals and their periods are in general agreement with observations [*Sturges*, 1993; *Sturges and Leben*, 2000]; the observations show dominant eddy shedding frequency of 6, 9 and 11 months. However, Sturges and Leben's analysis was based on 26 years of data, from 1973 to 1999, while the model analysis is based on only a four-year simulation; a more quantitative comparison with much longer simulation period (16 years) is contained in Oey and Lee (submitted manuscript, 2002b).

[16] We now further investigate the nature of the EOF modes, describe above, in order to identify how each mode relates to the modeled flow parameters in the YC.

3.2.1. EOF Mode 1: "The Meander Mode"

[17] The spatial structure of the first mode, with maximum variability near the edges of the surface inflow, suggests to us that the first mode may be related to fluctuations in the upper flow position. A time series representing the east-west variations in the position of the inflow is obtained from the location of the 40 cm s^{-1} contour at sigma level 6. This contour approximately represents the eastern edge of the inflow in Figure 4a, and is close to the center of the YC at about 65 m below the surface. The power spectrum of this time series (Figure 13a)

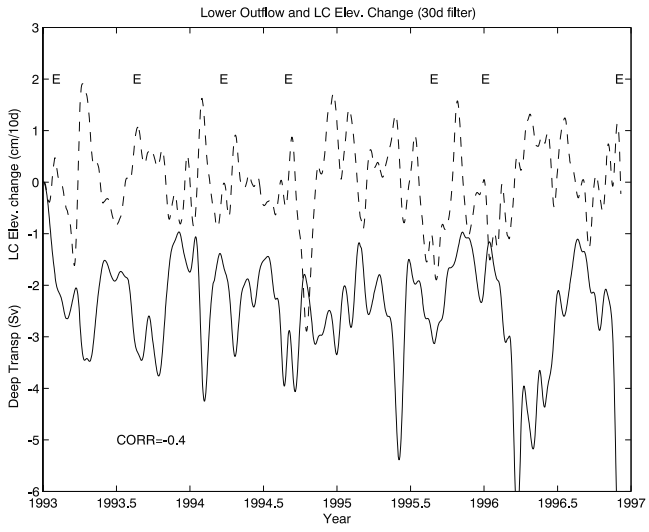

Figure 9. Outflow transport below 800 m (solid line, in Sv) and area averaged surface elevation change (dashed line, in cm change per 10 days). Both time series were smoothed by a 30-days low-pass filter. Correlation coefficient is −0.4.

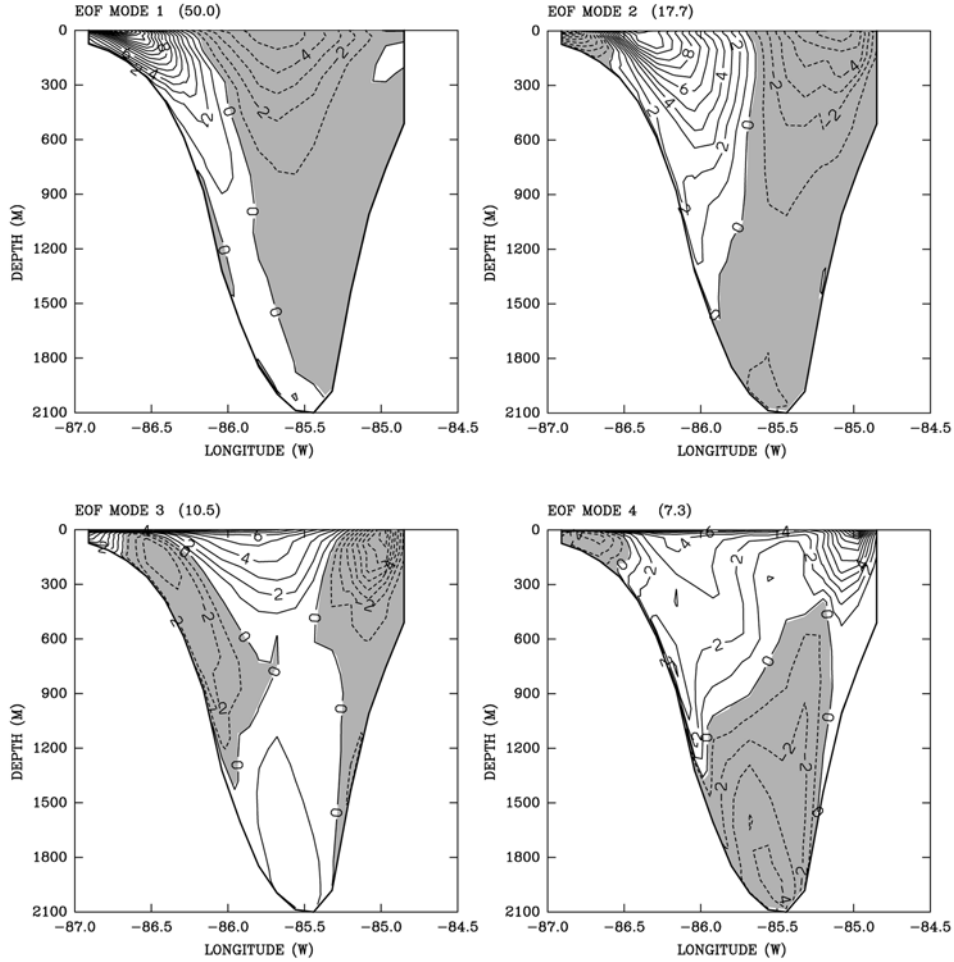

Figure 10. The spatial structure of the first four Empirical Orthogonal Functions (EOF) Modes of the along-channel flow (the percent of variability represented by each mode is indicated in parentheses). Shaded areas and dashed contours represent negative values; each contour represents 1/100th of the normalized amplitude value.

shows that most of the peaks in the inflow position time series are also found in the spectrum of EOF mode 1 (Figure 12a), including peaks at 34, 47, 60, 73, 93 and 171 days (the peaks of 256 and 341 days merge into one peak in both spectra). While the time series are not long enough for calculations of the significance and coherencies of the long-term peaks, which are the main interest here, a plot of both time series (Figure 14) and direct linear regression calculation, with a correlation coefficient = 0.83, show that the two are correlated on short- and long-term periods. However, direct relation between the time evolution of mode 1 and eddy shedding events is not clear and their correlation is not statistically significant. Only two of the seven shed eddies seem to coincide with an eastward shift in the inflow, with the clearer example at the beginning of 1996 (Figure 5), and possibly also in late 1994. An indirect effect of LC meander on eddy shedding is by its influence on the return transports (e.g., Figure 5) and possibly also it may trigger the development of propagating meanders further north into the Gulf. As will be shown next, changes in inflow transport (which correlates with the return transport) do seem to affect eddy shedding.

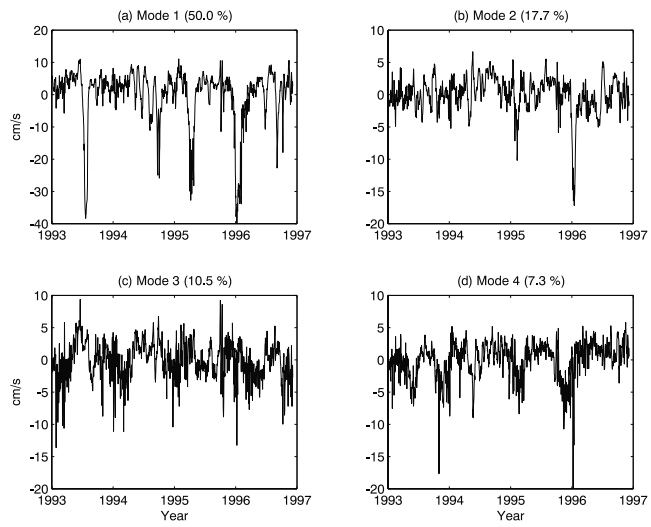

Figure 11. The temporal variations of the first four EOF Modes shown in Figure 10.

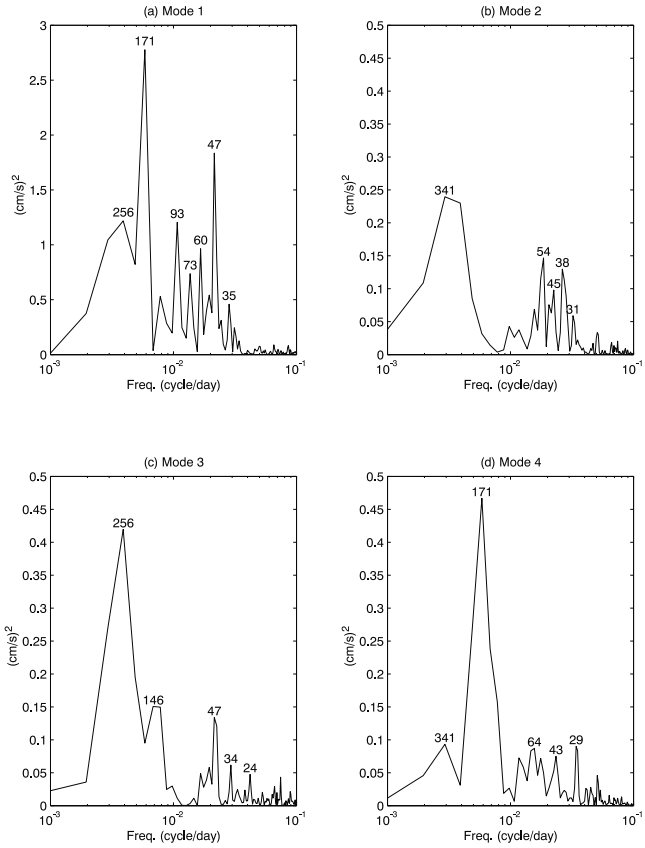

Figure 12. Power spectra of the time evolution of the first four EOF Modes shown in Figure 11. The period (in days) of the most energetic peaks are indicated.

3.2.2. EOF Mode 2: "The Transport Mode"

[18] The spatial structure of mode 2 (Figure 10) resembles the structure of the mean flow, especially in the upper layers (Figure 4a). This suggests that mode 2 may relate to the inflow transport in Figure 8b. Indeed, the spectrum of the inflow transport (Figure 13b) shows an energetic peak at

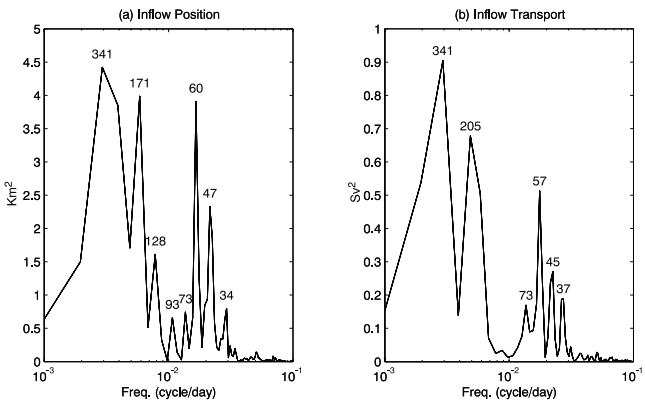

Figure 13. Power spectra of (a) the east-west variation in the position of the inflow core defined by the location of the 40 cm s^{-1} contour at sigma level 6 (about 65 m below the surface, see Figure 4), and (b) the inflow transport (the solid line in Figure 8b). The period (in days) of the most energetic peaks are indicated.

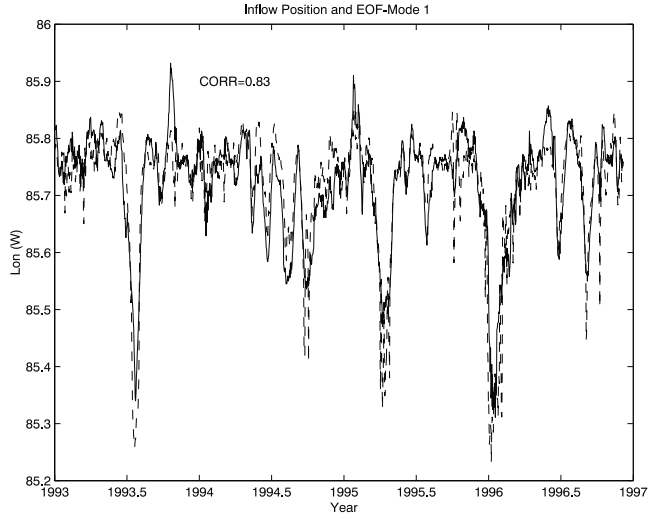

Figure 14. A comparison of the east-west variations in the position of the inflow core across the YC (solid line) and the time evolution of EOF mode 1 (dashed line). The amplitude of the EOF mode (see Figure 11a) is scaled to fit the longitude units of the flow position. The correlation coefficient between the two time series is 0.83.

341 days, at the same period as the most energetic peak in mode 2. Figure 15 compares the time evolution of mode 2 with the transport of the upper inflow. The correlation coefficient is 0.7. A 30-day low-pass filter was applied in Figure 15 to remove high frequencies. Without the filter, the correlation coefficient is smaller, 0.5, but is still significant at the 95% confidence level. Eddy shedding events are also marked in Figure 15; almost all the eddy shedding events occurred when inflow transport has increased and is near its

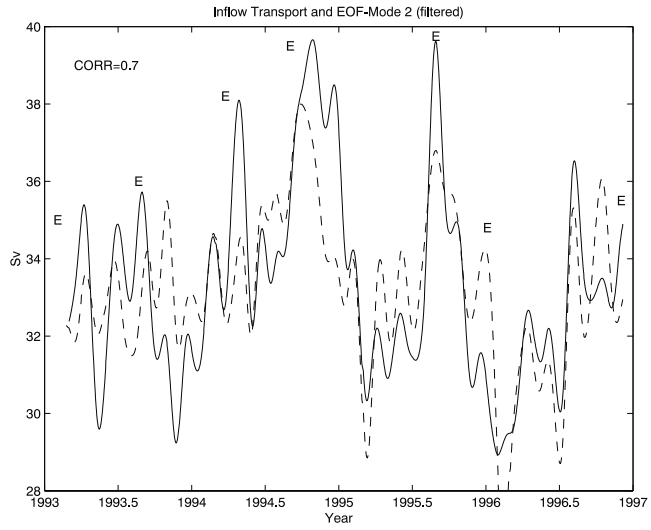

Figure 15. A comparison of the variations in the inflow transport (the solid line of Figure 8b) (solid line) and the time evolution of EOF mode 2 (dashed line). The amplitude of the EOF mode (see Figure 11b) is scaled to fit the units (Sv) of the transport. The time series were smoothed with a 30-day low-pass filter. The correlation coefficient between the two time series is 0.7.

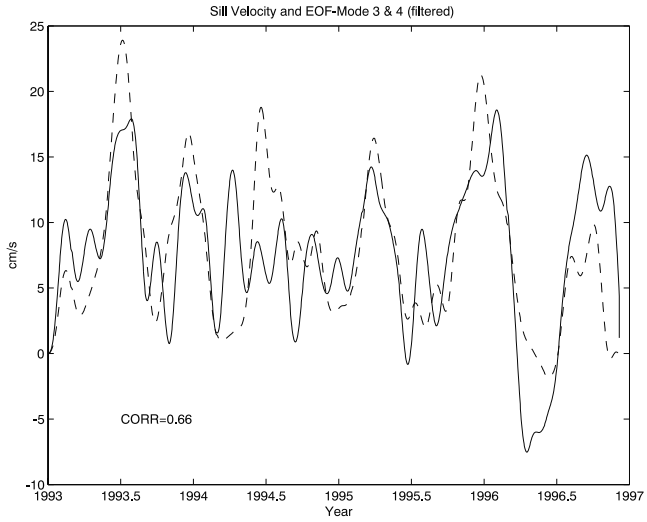

Figure 16. A comparison of the model v-velocity component at the center of the section in Figure 4, at 150 m above the sill (solid line), and the sum of mode 3 and mode 4 (dashed line). The sign of mode 4 has been reversed and the amplitude of the sum of the modes was scaled to fit the units and sign of the velocity record. The time series were smoothed with a 30-day low-pass. The correlation coefficient between the two time series is 0.66.

peak. One clear exception where the peak in transport is relatively small when an eddy was shed is at the beginning of 1996, which coincides with the extreme eastward shift in the inflow position and in the time evolution of EOF mode 1, as discussed before (Figure 14). The fact that fluctuations in the inflow transport appear to correlate with eddy shedding events is perhaps not surprising, since each eddy shedding requires additional inflow transport to allow expansion of the LC. This result is also consistent with the correlation between LC extension and deep transport (Figure 9), since in our model (as well as in *Oey* [1996]) the inflow and outflow transports are highly correlated with each other, but are in opposite directions.

3.2.3. EOF Modes 3 and 4: "The Maul Modes"

[19] We look at these two modes together, as these modes contain more variability near the deepest part at the center of the sill (mode 4 in particular) than the first two modes do. Modes 3 and 4 are compared with the model v velocity component 150 m above the bottom at the center of our section. The two modes seem to be out of phase with each other, as appear in their spatial structure (Figure 10) and temporal evolution (Figure 11), thus the combined time series is taken as $\Phi(t) = A_3\Phi_3(t) + A_4\Phi_4(t)$ with $(A_3, A_4) = (1, -1)$. The results below will eventually show that our choice of coefficients A_3 and A_4 was reasonable. The linear regression correlation between modes 3 and 4 and the sill velocity, with correlation coefficient = 0.66, and the comparison of the two time series (Figure 16), indicate that they correlate well. (A 30-day low-pass filter was applied; without the filter the correlation coefficient is smaller, still significant = 0.44). Attempts to correlate each individual mode separately or use different coefficients A_i yield much lower correlations. Therefore, the combined modes 3 and 4 represent the dominant fluctuations in the deepest part of the channel. Moreover, the power spectrum of the combined record of modes 3 and 4 in Figure 17 shows that the most energetic peak is at 205 day- the same period as the model and the Maul's observed spectra of Figure 3. We will call these two modes "the Maul modes" because of their close relation with the sill velocity and the apparent similarity in the time evolution of the two modes and the observed near-bottom velocity. Because these higher EOF modes are independent from the first two modes, which more directly relate to LC meanders and variations in upper channel transport, hence the LC extension, our results explain why *Maul et al.* [1985] did not find significant correlations between sill velocity (modes 3 and 4) and LC extension (mode 2 in particular).

4. Summary and Conclusions

[20] Recent observations [*Bunge et al.*, 2002; *Ochoa et al.*, 2001; *Sheinbaum et al.*, 2002] indicate more complex flow field and variability than previously thought based on more limited measurements [*Maul*, 1977; *Maul et al.*, 1985; *Burkov et al.*, 1982]. However, little is known about the nature of the forcing and the physical parameters that account for their variability. The aim of the study is therefore to analyze results from a high resolution numerical

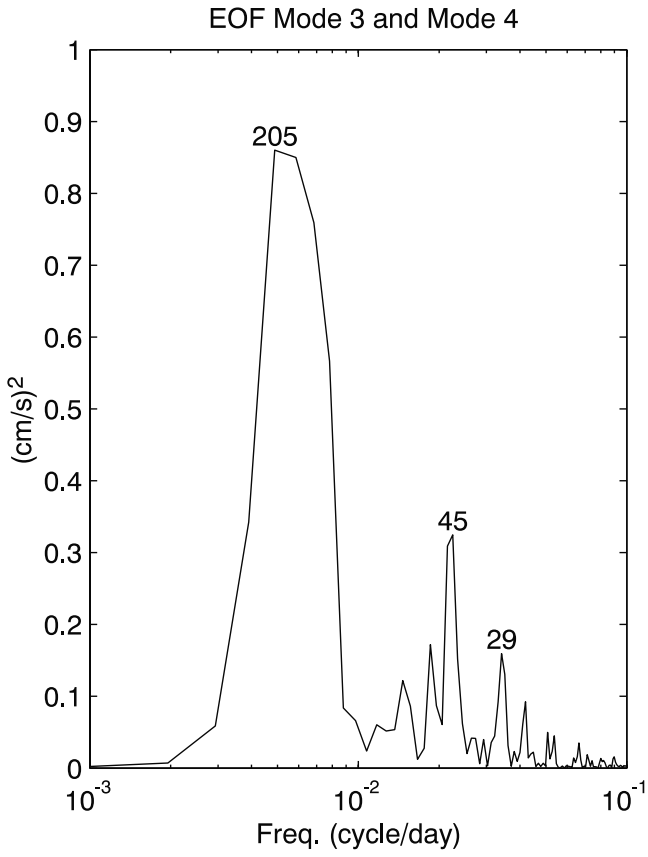

Figure 17. Power spectrum of the combined time evolution record of EOF modes 3 and 4 (unsmoothed). The period (in days) of the most energetic peaks are indicated. Note that the 205 days peak of the observed and model deep velocity over the sill (Figure 3) is reproduced by the combined EOF modes.

ocean model in order to describe the structure and variability of the flow through the YC, and to better understand how these relate to the forcing of LC variations and eddy shedding. The analysis of model results includes two parts. In the first part, a comparison was made between model results and published observations, in order to evaluate the overall statistics, e.g., mean and standard deviation of velocity and transports, of the flow. In the second part an EOF and coherency analysis were made in an attempt to identify the forcing and physical parameters responsible for the dominant modal fluctuations in the Channel.

[21] The model results indicate a highly variable flow field through the YC, in agreement with recent observations, in most aspects. The results show a flow field with four distinct cores: 1. An upper ocean inflow core with transport of 33 Sv and maximum mean flow of about 1.5 m s^{-1}, which is located near the western (Mexican) side of the YC, but occasionally shifts offshore on timescales of about 2, 6 and 11 months. 2. An upper ocean recirculation outflow core with transport of about 5.5 Sv and maximum mean flow of about 0.25 m s^{-1}, which is located near the eastern (Cuban) side of the YC. 3. A deep boundary undercurrent along the western slope with mean southward velocity of 0.17 m s^{-1}. 4. A deep boundary undercurrent along the eastern slope with mean southward velocity of 0.1 m s^{-1}. The total deep return currents combined to an outflow mean transport of about 2.5 Sv, but occasionally return deep transports are as large as 5–10 Sv. One discrepancy between the model results and the new observations [*Ochoa et al.*, 2001; *Sheinbaum et al.*, 2002] is that, the model shows a more extended return flow near the surface on the eastern side of the Channel than the observations do. Because of the large interrannual variability of the flow in this area, and the limited period of observations (<2 years) a much longer observed record is probably needed in order to verify the exact nature of this feature. Ongoing simulations with data assimilation during the period coincident with that observed (not shown here), do indicate a weaker eastern return flow, more similar to the observations. The total net transport across the Channel in the present model, 25.3 Sv, is in good agreement with recent observed estimates of a mean transport of 25 Sv [*Ochoa et al.*, 2001] or 23.8 [*Sheinbaum et al.*, 2002]. Previous estimates in the YC cited a larger mean transport of 28–30 Sv [*Schmitz and Richardson*, 1991; *Schmitz and McCartney*, 1993; *Johns et al.*, 2002].

[22] When the LC volume increases the upper inflow increases, and thus the deep return flow must increase, as proposed by *Maul* [1977], *Maul et al.* [1985], and recently observed by *Bunge et al.* [2002]. This relation is confirmed in our calculations- a significant linear correlation was found between changes in the extension of the LC and the total deep return flow below 800 m. Pulses of strong return deep flows coincide with large increase in LC volume; such pulses usually occur between eddy shedding events when the LC is growing and are mostly confined to the west and east deep slopes of the channel. The results are consistent with the early simulations using a smaller domain [*Oey*, 1996], thus suggesting that the inflow/outflow relation in the YC is largely controlled by local dynamics.

[23] An EOF analysis explores the spatial structure of the first four modes and their temporal evolution. The first four EOF modes accounts for 50%, 18%, 11% and 7%, respectively, of the variability. The EOF mode#1 of the along-channel currents is surface-trapped, is 180° out of phase across the channel, and correlates well (correlation coefficient $\gamma \approx 0.8$) with the cross-channel vacillations of the LC frontal position. Its time series at times visually correlates also with the inflow transport and LC eddy-shedding events (e.g., Figure 5) but the correlation is not statistically significant. The EOF mode#2 has a spatial structure that mimics that of the mean flow: dominated by two vertically more coherent regions that are 180° out of phase across the Channel. The mode is dominated by two periods, approximately 11 months and 2 months respectively, and correlates ($\gamma \approx 0.7$) with the inflow transport. This mode seems to directly relate to eddy shedding events; six of the seven eddies shed during the 4-year simulation occurred near a peak in the inflow transport, the seventh eddy shed near a peak in mode#1 and an extreme eastward shift in the position of the inflow. The time series of the combined EOF mode#3 and mode#4 together correlates ($\gamma \approx 0.66$) with the deep current over the sill, and is dominated by fluctuations with a period $\approx$ 205 days coincident with the dominant low-frequency fluctuations inherent in *Maul et al.* [1985] sill measurement. The higher modes (#3 and #4) account for most of the velocity variability in the deep layers over the center of the sill.

[24] Following the above description of the EOF modes in the Yucatan Channel, we suggest naming these EOF modes "the meander mode" (mode 1), "the transport mode" (mode 2), and "the Maul modes" (modes 3 and 4). While we clearly identified the long-term modes of variability, more analysis is needed to understand the various high frequency oscillations evident in the observed and the simulated records.

[25] Our results may help to explain why *Maul et al.* [1985] could not find a significant correlation between the near-bottom velocity at the center of the sill and variations in the LC expansion. First, the location of the Maul's current meter was at the center of the sill while most of the deep outflow (in the model and in the new observations) is on the side slopes of the channel. Second, the so-called "Maul modes" (EOF modes 3 and 4) do not correlate with the LC meander mode (EOF mode 1), nor with the transport mode (EOF mode 2).

[26] An important question is whether or not variations in the YC flow affect the frequency of LC eddy shedding (see Oey and Lee, submitted manuscript, 2002). Do the most energetic peaks in the YC EOF modes, 5.6 months, 8.4 months and 11.2 months, relate to the frequency of LC eddy shedding? Unfortunately, our simulations are not long enough to obtain a reliable statistics of eddy shedding frequency in the model, as has been done by *Sturges and Leben* [2000] from analysis of 26 years of observations which show dominant eddy shedding frequencies of 6, 9 and 11 months. During the four-year period analyzed here, seven LC eddies were shed at irregular time intervals of 6.6, 7.1, 5.3, 11.9, 4.2 and 10.9 months, thus suggesting that there is a relation between the EOF modes and eddy shedding events. This relation has been established to some extent for the EOF mode#2 and the variations in the inflow transport, but it is less clear for other modes.

[27] Note that the present simulation produces irregular LC eddy-shedding periods. *Oey* [1996] shows that irregular eddy shedding in an ocean model depends on horizontal viscosity. Here, we provide an additional mechanism- forcing by wind-driven transport variations. In Oey and Lee (submitted manuscript, 2002) we find that without the ECMWF wind a regular LC eddy-shedding ensue and that irregular shedding occurs as a result of fluctuating YC transports forced by variations in the wind and caribbean eddies. Therefore, while the basic dynamics in the YC may be controlled internally by local topography and stratification, wind (local and remote) and eddies can play an important role in affecting LC and eddy shedding frequency.

[28] **Acknowledgments.** The study is supported by the Mineral Management Service under contracts 1435-0100-31076, 1435-0001-30787 and 01-99-31028 (via SAIC). T.E is also supported by the Office of Naval Research, award N00014-00-1-0228. Computational resources were provided by the NOAA/GFDL super computer facilities.

References

Baringer, M. O., and J. C. Larsen, Sixteen years of Florida Current transport at 27°N, *Geophys. Res. Let.*, *28*, 3179–3182, 2001.

Blumberg, A. F., and G. L. Mellor, A description of a three-dimensional coastal ocean circulation model, in *Three-Dimensional Coastal Ocean Models*, *Coastal Estuarine Stud.*, vol. 4, edited by N. S. Heaps, pp. 1–16, AGU, Washington, D.C., 1987.

Bretherton, C. S., C. Smith, and J. M. Wallace, An intercomparison of methods for finding coupled patterns in climate data, *J. Clim.*, *5*, 541–560, 1992.

Bunge, L., J. Ochoa, A. Badan, J. Candela, and J. Sheinbaum, Deep flows in the Yucatan Channel and their relation to changes in the Loop Current extension, in press, *J. Geophys. Res.*, *107*(C12), 3233, doi:10.1029/2001JC001256, 2002.

Burkov, V. A., L. I. Galerkin, and A. B. Zubin, New data on water exchange through the Yucatan Strait (in Russian), *Dokl. Akade. Nauk USSR*, *265*, 190–195, 1982. (*Oceanology*, Engl. Transl., 198–200, 1984.)

Ezer, T., Can long-term variability in the Gulf Stream transport be inferred from sea level?, *Geophys. Res. Lett.*, *28*, 1031–1034, 2001.

Hurlburt, H. E., and J. D. Thompson, A numerical study of Loop Current intrusions and eddy shedding, *J. Phys. Oceanogr.*, *10*, 1611–1651, 1980.

Johns, W. E., T. L. Townsend, D. M. Fratanton, and W. D. Wilson, On the Atlantic inflow to the Caribbean Sea, *Deep Sea Res.*, *49*, 211–243, 2002.

Maul, G. A., The annual cycle of the Gulf Loop Current, Part I, Observations during a one-year time series, *J. Mar. Res.*, *35*, 29–47, 1977.

Maul, G. A., D. A. Mayer, and S. R. Baig, Comparisons between a continuous 3-year current-meter observation at the sill of the Yucatan Strait, satellite measurements of Gulf Loop Current area, and regional sea level, *J. Geophys. Res.*, *90*, 9089–9096, 1985.

Mellor, G. L., and T. Yamada, Development of a turbulent closure model for geophysical fluid problems, *Rev. Geophys.*, *20*, 851–875, 1982.

Murphy, S. J., H. E. Hurlburt, and J. J. O'Brien, The connectivity of eddy variability in the Caribbean Sea, the Gulf of Mexico, and the Atlantic Ocean, *J. Geophys. Res.*, *104*, 1431–1453, 1999.

Ochoa, J., J. Sheinbaum, A. Baden, J. Candela, and D. Wilson, Geostrophy via potential vorticity inversion in the Yucatan Channel, *J. Mar. Res.*, *59*, 725–747, 2001.

Oey, L.-Y., Simulation of mesoscale variability in the Gulf of Mexico: Sensitivity studies, comparison with observations, and trapped wave propagation, *J. Phys. Oceanogr.*, *26*, 145–175, 1996.

Oey, L.-Y., and P. Chen, A model simulation of circulation in the northeast Atlantic shelves and seas, *J. Geophy. Res.*, *97*, 20,087–20,115, 1992.

Oey, L.-Y., and H.-C. Lee, Deep eddy energy and topographic Rossby waves in the Gulf of Mexico, *J. Phys. Oceanogr.*, *32*, 3499–3527, 2002.

Schmitz, W. J., Jr., and M. S. McCartney, On the North Atlantic circulation, *Rev. Geophys.*, *31*, 29–49, 1993.

Schmitz, W. J., Jr., and P. L. Richardson, On the sources of the Florida Current, *Deep Sea Res.*, *38*(Suppl. 1), 379–409, 1991.

Sheinbaum, J., J. Candela, A. Badan, and J. Ochoa, Flow structure and transports in the Yucatan Channel, *Geophys. Res. Let.*, *29*(3), 1040, 10.1029/2001GL0139990, 2002.

Smagorinsky, J., General circulation experiments with the primitive equations, I, The basic experiments, *Mon. Weather Rev.*, *91*, 99–164, 1963.

Sturges, W., The frequency of ring separations from the Loop Current, *J. Phys. Oceanogr.*, *24*, 1647–1651, 1993.

Sturges, W., and B. G. Hong, Gulf Stream transport variability at periods of decades, *J. Phys. Oceanogr.*, *31*, 324–332, 2001.

Sturges, W., and R. Leben, Frequency of ring separations from the Loop Current In the Gulf of Mexico: A revised estimate, *J. Phys. Oceanogr.*, *30*, 1814–1818, 2000.

Sturges, W., J. C. Evans, W. Holland, and S. Welsh, Separation of warm-core rings in the Gulf of Mexico, *J. Phys. Oceanogr.*, *23*, 250–268, 1993.

Teague, W. J., M. J. Carron, and P. J. Hogan, A comparison between the Generalized Digital Environmental Model and Levitus climatologies, *J. Geophy. Res.*, *95*, 7167–7183, 1990.

Wang, D.-P., L.-Y. Oey, T. Ezer, and P. Hamilton, The near-surface currents in DeSoto Canyon (1997–1999): Observations, satellite data, and comparison with model simulations, *J. Phys. Oceanogr.*, *33*, 313–326, 2003.

Welsh, S. E., and M. Inoue, Loop Current rings and the deep circulation in the Gulf of Mexico, *J. Geophys. Res.*, *105*, 16,951–16,959, 2000.

T. Ezer, H.-C. Lee, and L.-Y. Oey, Program in Atmospheric and Oceanic Sciences, P.O. Box CN710, Sayre Hall, Princeton University, Princeton, NJ 08544-0710, USA. (ezer@splash.princeton.edu; lhc@splash.princeton.edu; lyo@splash.princeton.edu)

W. Sturges, Department of Oceanography, Florida State University, Tallahassee, FL 32306, USA. (sturges@ocean.ocean.fsu.edu)